Assessing CMIP6 uncertainties at global warming levels

Guillaume Evin, Aurélien Ribes, Lola Corre

Assessing CMIP6 uncertainties at global warming levels

Guillaume Evin

guillaume.evin@inrae.fr

IGE: Institut des Geosciences de l'Environnement https://orcid.org/0000-0003-3456-9441

Aurélien Ribes

CNRM GMGEC: Centre National de Recherches Meteorologiques Groupe de Meteorologie de Grande Echelle et Climat

Lola Corre

Meteo France

Research Article

Keywords: Climate change, Uncertainty, Warming level, CMIP6

Posted Date: March 13th, 2024

DOI: https://doi.org/10.21203/rs.3.rs-4013273/v1

Assessing CMIP6 uncertainties at global warming levels

Guillaume Evin[1*], Aurélien Ribes[2] and Lola Corre[3]

[1*]Univ. Grenoble Alpes, INRAE, CNRS, IRD, Grenoble INP, IGE, Grenoble, 38000, France.
[2]Centre National de Recherches Météorologiques, Université de Toulouse, Météo-France, CNRS, Toulouse, France.
[3]Centre National de Recherches Météorologiques, Université de Toulouse, Météo-France, CNRS, Toulouse, France.

*Corresponding author(s). E-mail(s): guillaume.evin@inrae.fr;
Contributing authors: aurelien.ribes@meteo.fr; lola.corre@meteo.fr;

Abstract

IPCC reports and climate change impact studies generally exploit ensembles of climate projections based on different socio-economic pathways and climate models, which provide the temporal evolution of plausible future climates. However, The Paris Agreement and many national and international commitments consider adaptation and mitigation plans targeting future global warming levels. Model uncertainty and scenario uncertainty typically affect both the crossing-time of future warming levels and the climate features at a given global warming level. In this study, we assess the uncertainties in a multi-model multi-member CMIP6 ensemble (MME) of seasonal and regional temperature and precipitation projections. In particular, we show that the uncertainties of regional temperature projections are considerably reduced if considered at a specific global warming level, with a limited effect of the emission scenarios and a reduced influence of GCM sensitivity. We also describe in detail the large uncertainties related to the different behavior of the GCMs in some regions.

Keywords: Climate change, Uncertainty, Warming level, CMIP6

1 Introduction

A critical issue in climate change studies is the estimation of uncertainties in projections along with the contribution of the different uncertainty sources, including scenario uncertainty, the different components of model uncertainty, and internal variability (see, e.g., Hawkins and Sutton, 2009). Scenario uncertainty is related to the possible evolution of greenhouse gas emissions, which are implemented by a limited number of socio-economic evolutions and related greenhouse gas emissions (e.g. the Shared Socioeconomic Pathways, SSPs, in the last IPPC reports). Model uncertainty corresponds to the dispersion between the different climate responses obtained with different models (e.g. Global Climate Models, GCMs) for the same forcing configuration. Internal variability is due to the chaotic variability of the climate (Deser et al, 2012).

Over the recent years, uncertainty in climate projections has been mostly explored and partitioned based on Multi-model Multi-member Ensembles (MMEs) of transient climate projections. Various methods have been proposed for this, most of them based on an Analysis of Variance (ANOVA) applied for different future time periods (Hawkins and Sutton, 2009; Yip et al, 2011; Paeth et al, 2017; Evin et al, 2019). Instead of assessing the temporal evolution of climate variables, many recent studies, the IPCC special report on the impacts of global warming of 1.5°C (IPCC, 2018) and the Working Group I contribution to the AR6 (see, e.g. chapter 11, IPCC, 2021) investigate the impacts of climate change according to certain reference levels of global warming level (e.g. +1.5°C or +2°C above pre-industrial levels at the planetary scale), hereafter denoted as GWL. Indeed, many national and international commitments to reduce emissions, such as the Paris Agreement, target a precise level of global warming which must not be exceeded.

Different approaches have been proposed to estimate projected changes as a function of the GWLs (Schleussner et al, 2016; Seneviratne et al, 2016; Wartenburger et al, 2017; Baker et al, 2018; Dosio and Fischer, 2018; Nikulin et al, 2018; Sun et al, 2019). James et al (2017) provide a detailed critical review of the different existing approaches targeting specific GWLs based on available MMEs. A straightforward approach consists of selecting a future 30-year period corresponding to the desired GWL for one forcing scenario or comparing the impact of different warming levels by comparing climate simulations obtained with different forcing scenarios (e.g. at the end of the century). However, simulations obtained with different models with the same forcing scenario have different global temperature responses (so-called climate sensitivity, see e.g. Mauritzen et al, 2017) so that a warming level corresponds to different time windows according to the GCM (Scafetta, 2021). To account for the climate sensitivity of the climate model, a simple solution is to choose a different time slice for each model (Vautard et al, 2014; Schleussner et al, 2016; Nikulin et al, 2018). In any case, the choice of a future time window has the major drawback of being subject to multi-decadal natural variability (Lehner and Deser, 2023) which leads to large uncertainties in both the estimation of the GWL and the related impacts (i.e. regional variables). Pattern scaling is another popular approach that exploits existing MMEs to relate GWLs to local responses to climate change (Tebaldi and Arblaster, 2014; Herger et al, 2015; Tebaldi and Knutti, 2018). This approach applies linear regressions between the regional/local variable of interest and GWLs, the slope of the regression providing a direct estimate of the regional/local response per degree of GWL. An important advantage of this approach is to dampen the influence of natural variability. These linear relationships seem to be acceptable for seasonal temperature averages, less adapted for seasonal precipitation averages (Tebaldi and Arblaster, 2014), and limited for other variables (Lopez et al, 2014). Different initiatives have also been proposed to run climate simulations explicitly designed to target specified warming levels (Mitchell et al, 2017; Schleussner et al, 2018; Sun et al, 2019).

This study proposes to adapt the Quasi-Ergodic ANOVA (QEANOVA) framework considered in several previous studies (Hawkins and Sutton, 2009; Hingray and Saïd, 2014; Evin et al, 2019) to assess the evolution of the climate responses and the different uncertainties as a function of GWLs. The proposed approach builds upon the strengths of the "Time sampling" and "Pattern scaling" approaches and applies smoothing splines with high smoothing parameters to relate robust estimates of GWLs (obtained from different forcing scenarios and GCMs) to robust estimates of the climate responses to climate change. This approach, by construction, shares the same limitation as the "pattern scaling" and "time sampling" approaches in that it assumes the climate response to a specific warming level is independent of the emission trajectory whereas regional changes can be sensitive to the rate of warming, lags in the climate system, emissions reductions, or temperature overshoot (James et al, 2017). Typical examples of changes sensitive to the rate of warming include long-term sea level changes (Schaeffer et al, 2012), ice cover (Gregory et al, 2004), or temperature-sensitive biophysical systems (e.g. coral reefs, Frieler et al, 2013).

The current study aims to assess different uncertainties of the last Coupled Model Intercomparison Project exercise (CMIP6) using a large MME of seasonal and regional temperature and precipitation projections. One main objective of this study is to provide a detailed understanding of the model uncertainties for this MME for a specific warming level. The objectives are:

- to illustrate that projected changes of seasonal temperature evolve roughly linearly as a function of global warming, for this CMIP6 multi-model multi-member ensemble (MME), in line with previous studies (Tebaldi and Arblaster, 2014), but not at the same rate for the different GCM, and have contrasted monotonic evolution for seasonal precipitation,
- to present the spatial variability of these projected changes, and the corresponding uncertainties (total uncertainty of the ensemble, GCM, and scenario uncertainties),

- to show that GCM and scenario uncertainties for projected seasonal temperatures are smaller when assessed as a function of global warming, compared to standard uncertainty assessment as a function of time. In this case, the proposed approach reconciles climate simulations obtained with different emission scenarios and with GCMs having different climate sensitivity,
- to identify the regions (Arctic Ocean, Sahel) and seasons where projected changes of seasonal temperature and precipitation are highly sensitive to the choice of the GCM/SSP scenario. The particular behavior of some GCMs is highlighted in comparison to the other GCMs of the MMEs.

Section 2 presents the MME used in this study, which is based on three different emission scenarios and seven CMIP6 GCMs. For each scenario/GCM combination, between five and ten members are used to provide projections of mean temperature and precipitation for winter and summer seasons. Section 3.2 presents the methodology applied in this paper, which follows up the so-called QUALYPSO approach applied in Evin et al (2019); Bichet et al (2020); Evin et al (2021). Section 4 presents the mean climate change response obtained with this CMIP6 MME for a warming level of 2°C and for the IPPC WGI reference regions, as well as the corresponding uncertainties, and discuss these results in comparison to the materials presented in the literature. Section 5 then describes the spatial patterns of GMC uncertainty and the different responses of each GCM to a warming level of 2°C concerning seasonal temperature and precipitation changes. Section 6 then quantifies the decrease of the GCM uncertainties that can be attributed to the GCM sensitivity, by comparing the uncertainties for a warming level of 2°C to the uncertainties around 2038, which corresponds to a mean warming level of +2°C. Section 7 discusses different aspects related to this study and concludes.

2 CMIP6 climate projections

This study exploits climate projections from seven CMIP6 GCMs driven by three Shared Socioeconomic Pathways (SSPs, Riahi et al, 2017) which cover a wide range of projected warming levels: SSP2-4.5, SSP3-7.0, and SSP5-8.5. Table 1 indicates the list of selected GCMs and the corresponding number of members selected for each GCM and SSP scenario (see Table S1 in the Supplement for the corresponding lists of members). We also indicate the corresponding Transient climate response (TCR) as provided in a supplement of Chapter 7 / WGI of the IPCC AR6 report (IPCC, 2021)[1]. This ensemble has been selected according to three criteria:

- Model independence: As illustrated by Brunner et al (2020), most of the CMIP6 GCMs share important similarities in terms of model structure, implementation, and parameterization. Here, the selected models avoid important model redundancy indicated in Figure 5 of Brunner et al (2020). One exception is ACCESS-CM2 and UKESM1-0-LL which are similar and reach high warming levels. Both are kept in this study because they do not necessarily lead to the same responses to climate change.
- Range of TCR: The selected GCMs cover a wide range of TCR, from low TCR values (MIROC6) to the highest TCR values among the CMIP6 GCMs (ACCESS-CM2, UKESM1-0-LL).
- Number of members: A minimum of five members are required for each GCM and SSP scenario. Several models (e.g. NorEMS2-MM, CESM2, EC-Earth3) could not be included because they did not have enough members for the three SSP scenarios and for the two variables investigated in this study: near-surface air temperature ('tas') and precipitation ('pr').

At the end, we select seven GCMs. For each GCM/SSP scenario, the maximum number of members was limited to 10 which was deemed sufficient to obtain a fair

[1] https://www.ipcc.ch/report/ar6/wg1/downloads/report/IPCC_AR6_WGI_Chapter07_SM.pdf

representation of the interannual variability of projected changes. In total, 177 simulations of temperature and precipitation for the period 1850-2100 have been downloaded at a monthly scale, and regridded onto a common 1° × 1° degree global grid using a bilinear interpolation (cdo command `cdo -remapbil,r360x180`). These ensembles are then aggregated temporally, for winter (DJF), spring (MAM), summer (JJA), and autumn (SON) seasons, and spatially, over the 58 AR6-WGI Reference Regions (Iturbide et al, 2020).

GCM	Number of members for each GCM/SSP scenario			TCR °C
	SSP2-4.5	SSP3-7.0	SSP5-8.5	
ACCESS-CM2	5	5	10	2.10
CanESM5	10	10	10	2.74
CNRM-ESM2-1	10	5	5	1.86
IPSL-CM6A-LR	7	10	5	2.32
MIROC6	10	10	10	1.55
MPI-ESM1-2-LR	10	10	10	1.84
UKESM1-0-LL	10	10	5	2.79

Table 1 Ensemble of CMIP6 climate projections selected in this study: Name of the GCM, number of members selected for each GCM/SSP scenario and Transient climate response (TCR) as provided by the IPCC AR6 report (see Table 7.SM.5 in IPCC, 2021).

3 Methods

3.1 Global warming levels for each GCM

Climate simulations obtained from GCMs can be used to compute average temperatures at the planetary level. In this study, the global mean surface temperatures (GMST) are averaged at an annual temporal scale over the period 1850-2014 for the historical runs, and for the period 2015-2100 with the different SSPs, for each GCM and the different members. These raw GMST values are smoothed using cubic splines (implemented by the function `smooth.spline` in R software) with the `df` argument of `smooth.spline` equal to 6, following the choices motivated by Rigal et al (2019);

Ribes et al (2022). This high smoothing parameter greatly dampens the effect of internal variability. These smoothed GMST values simulated by each GCM g and for an emission scenario s (historical or SSP) are denoted by $GMST_{g,s}(t)$ for a year t and can be compared to observed GMST values from HadCRUT5 (Morice et al, 2021) which provides a gridded dataset of GMST anomalies relative to the reference period 1961-1990. For the sake of comparison with absolute GMST values from the GCMs, a rough estimate of 14°C can be considered for the observed GMST for the period 1961-1990 (Jones et al, 1999). These observed GSMTs obtained from HadCRUT5 are also smoothed using cubic splines. Fig. 1a shows the different GMST for the seven GCMs of our ensemble, for the three emission scenarios. For the period 1850-1900, the smoothed GMST values $GMST_{g,s}(t)$ vary from 12.5°C to 14.5°C, while HadCRUT5 provides in-between GMST values. These first-order discrepancies can be observed for the entire period 1850-2100.

In this study, GMST anomalies relative to the pre-industrial period 1850-1900 are considered, in agreement with the IPCC special report on Global Warming of 1.5°C (IPCC, 2018). These GMST anomalies are referred to as global warming levels (GWLs) hereafter (or simply warming levels), and denoted by $GWL_{g,s}(t)$ for a GCM g and a year t. Figure 1b shows $GWL_{g,s}(t)$ for the different GCMs and the different emission scenarios. By construction, all $GWL_{g,s}(t)$ values are in agreement for the period 1850-1900. Some models seem to be colder during the period 1950-2000, which was identified as an overly strong negative aerosol forcing for UKESM1-0-LL (Mulcahy et al, 2023). For future periods, the warming level reached by the different climate projections depends on the SSP scenarios and the climate sensitivity of each GCM.

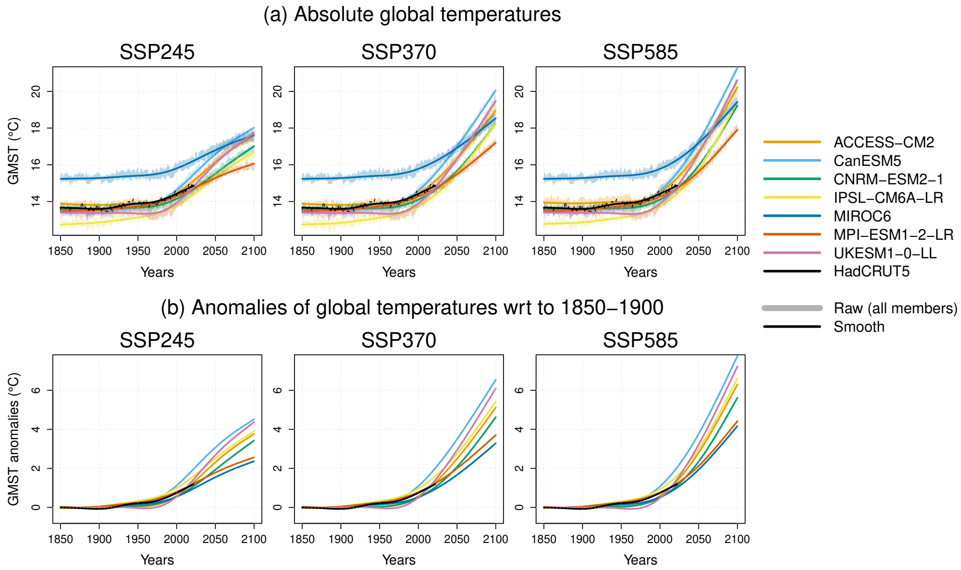

Fig. 1 Global temperatures from the GCMs and HadCRUT5. (a) Intervals covered by the different members of each GCM and the corresponding smooth GMST values $GMST_{g,s}(t)$ in degrees Celsius (one color by GCM). Raw and smoother HadCRUT GSMT values are shown with dash and plain black lines, respectively. (b) GMST anomalies (i.e. GWLs) $GWL_{g,s}(t)$) compared with the pre-industrial period 1850-1900.

3.2 Statistical assessment of mean changes and uncertainty sources

Mean changes and associated uncertainty components for the available MME are estimated using an ANalysis Of VAriance (ANOVA) with fixed effects applied to the ensemble of climate change responses estimated for the different chains. The climate change response of any given chain is considered to be a gradual and smooth function of the warming level, the deviations from the climate responses resulting from internal variability. The different steps are illustrated in Figure S1 in the Supplement for mean winter temperature in the AR6 reference region ARO (Arctic Ocean), for which the scenario uncertainty is particularly small despite large projected changes. The different steps of the approach can be summarized as follows:

- **Climate change response:** The climate change response $\phi_{g,s}(GWL)$ of a GCM g to an emission scenario s is obtained for different warming levels GWL for each of the 21 GCM/SSP combinations by fitting a trend model using a cubic smoothing spline to all members available for this GCM/SSP combination. In the same way as for the GMST estimates, high smoothing parameters (i.e. "equivalent degrees of freedom" `df`=6) are chosen to avoid spurious fluctuations in these fitted forced responses (see raw projections in Figs. S1a-c which can be compared to their respective climate responses in Figs. S1d-f). Figures S2-S9 in the Supplement show the raw projections and the corresponding climate responses for 11 illustrative reference regions, for the different seasons and variables.
- **Climate change response:** The climate change response $\phi^*_{g,s}(GWL)$ of any given scenario/GCM combination corresponds to the anomaly of the forced response for a given warming level GWL, and the forced response corresponding to the reference warming level of 0°C, i.e. the warming level considered as zero for the pre-industrial period 1850-1900. Absolute changes $\phi_{g,s}(GWL) - \phi_{g,s}(0)$ are considered for temperature, and relative changes $\phi_{g,s}(GWL)/\phi_{g,s}(0) - 1$ for precipitation (Figs. S1g-i).
- **Main ANOVA effects:** In QUALYPSO, the climate change response of a given simulation chain (a given emission scenario/GCM combination) is expressed as the sum of the grand ensemble mean, the main effects corresponding to the considered GCMs, and emission scenarios, and a residual term, i.e.:

$$\phi^*_{i,j}(GWL) = \mu(GWL) + \alpha_g(GWL) + \beta_s(GWL) + \xi_{g,s}(GWL), \qquad (1)$$

where

– $\mu(GWL)$ is the mean climate change response.

- $\alpha_g(GWL)$ and $\beta_s(GWL)$ are the main effects corresponding to the GCM g and emission scenario s, respectively, for a warming level GWL. They correspond to the deviations from the mean climate change response $\mu(GWL)$ (see illustration of $\mu(GWL)$ and $\mu(GWL) + \alpha_g(GWL)$ in Fig. S1j).
- $\xi_{g,s}(GWL) = \phi^*_{g,s}(GWL) - \mu(GWL) - \alpha_g(GWL) - \beta_s(GWL)$ is a residual term which represents the part of the climate change response that cannot be explained by the sum of the ensemble mean and the main effects. The variance of these residual terms $\xi_{g,s}(GWL)$ will be referred to as "Unexplained variance".

The decomposition (1) can be applied to a MME when different climate simulations are available for each scenario, GCM, for a warming level GWL. However, as illustrated in Fig. 1b, the warming levels reached by the different GCMs vary a lot for each SSP scenario. As a consequence, the decomposition (1) can only be obtained up to the maximum warming level shared by all climate simulations, i.e. 2.4°C for the SSP2-4.5, 3.4°C for the SSP3-7.0 and 4.2°C for the SSP5-8.5. In this study, we consider a partition of the uncertainties applied to 21 SSP/GCM simulation chains with the SSP2-4.5, SSP3-7.0, and SSP5-8.5 to obtain the uncertainty related to GCMs and emission scenarios, for warming levels GWL ranging from 0°C to 2°C. The different terms of Eq. 1 are estimated using a linear model implemented by the function `lm` in R ({R Core Team}, 2022). The dispersion (variance) between the main effects obtained for the seven GCMs and the three SSP scenarios gives an estimate of the GCM uncertainty and the scenario uncertainty, respectively (Fig. S1j-k), i.e. $V_{GCM}(GWL) = \mathbb{V}ar(\alpha_g(GWL))$ and $V_{SSP}(GWL) = \mathbb{V}ar(\beta_s(GWL))$. The unexplained variance is estimated as $\mathbb{V}ar(\xi_{g,s}(GWL))$. For each warming level GWL, the variances $V_{GCM}(GWL)$ and $V_{SSP}(GWL)$ can be tested against $\mathbb{V}ar(\xi_{g,s}(GWL))$ using F statistics to determine if the GCM and scenario effects can be considered as significantly different from zero.

The total variance is considered to be the sum of the three variance components, and the total uncertainty is defined as the standard deviation of the total variance, i.e.:

$$TU(GWL) = \sqrt{V_{GCM}(GWL) + V_{SSP}(GWL) + \mathbb{V}ar(\xi_{g,s}(GWL)}. \qquad (2)$$

In the following, we quantify mean changes and uncertainty sources for each IPPC WGI reference region and each element of the 1° × 1° grid. Applications are done on mean temperature and total precipitation aggregated for the different seasons. In this study, we focus on the results obtained at the scale of the reference regions for the winter (DJF) and summer (JJA) seasons but additional results are provided at the 1° × 1° resolution, and for the spring (MAM) and autumn (SON) seasons (see Section S5 in the Supplement).

4 Spatial variability of mean changes and related uncertainties

In this section, we first assess the mean climate change response obtained as the average of the climate change responses obtained for each of 21 GCM/SSP combinations (7 GCMs X 3 SSPs) and shown in Figs S2-S9 in the Supplement. Figure 2 shows the estimated mean climate change response of temperature and precipitation obtained for a warming level of 2°C compared with the pre-industrial period 1850-1900, for both winter and summer seasons. These maps exhibit clear regional contrasts which are very similar to the results shown in Figures 4.12 and 4.13 of the IPCC AR6 WGI report (IPCC, 2021) illustrating the projected changes of seasonal mean temperature and precipitation with the SSP3.7.0 for the period 2021-2040 (which corresponds roughly to the same warming level of +2°C). A GWL of +2°C leads to more than +7°C for winter temperature at high latitudes, i.e. the Arctic region and North of Russia. Land areas generally warm more than oceans and seas. These warming patterns are well understood and adequately represented by the climate models (IPCC, 2021). The mechanisms for the so-called Arctic amplification (e.g. surface-albedo feedback associated with the loss of sea ice and snow, lapse rate feedback) are for example described in Section 7.4.4.1 of IPCC (2021). Precipitation changes present large positive projected precipitation in the Arctic region in winter, and in the North of Africa and the Middle East in summer (up to +40%), and large negative precipitation changes in the North of Africa in winter, and Southern Europe, Central and South America, and South Africa in summer. Similar patterns are obtained in spring and autumn (see Fig. S13 in the Supplement), the strongest projected changes being obtained in autumn, up to +10.5°C and +42% for precipitation changes in the Arctic region. These large-scale responses are associated with stronger moisture transports, and modulated by the greater warming over land than ocean, atmospheric circulation responses, and land surface feedbacks (section 8.4.1.3 IPCC, 2021).

Figure 3 presents the total uncertainty at a warming level of +2°C and the different contributions (GCM, scenarios SSP, and unexplained variance) to the total variance for mean temperature and total precipitation in winter and summer. The total uncertainty of temperature changes is usually smaller than 0.4°C, except at high latitudes, especially where mean temperature changes are important (e.g. the Arctic Ocean) and potentially where the representation of the cryosphere is critical (e.g. Antarctica, Greenland, Arctic Ocean, Tibet), especially in winter. The total uncertainty of precipitation changes is also generally small (often less than 5% in ocean regions and less than 10% in land regions) but strong uncertainties are present in some specific regions (e.g. Western and North Africa for both seasons). Large uncertainties in arid regions (e.g. Sahel, Arabian Peninsula) are also obtained in spring and autumn (see Fig. S14 in the Supplement). These unstable projected changes of relative precipitation in dry regions can often be related to the small values of the seasonal precipitation obtained for the reference GWL (Bichet et al, 2020).

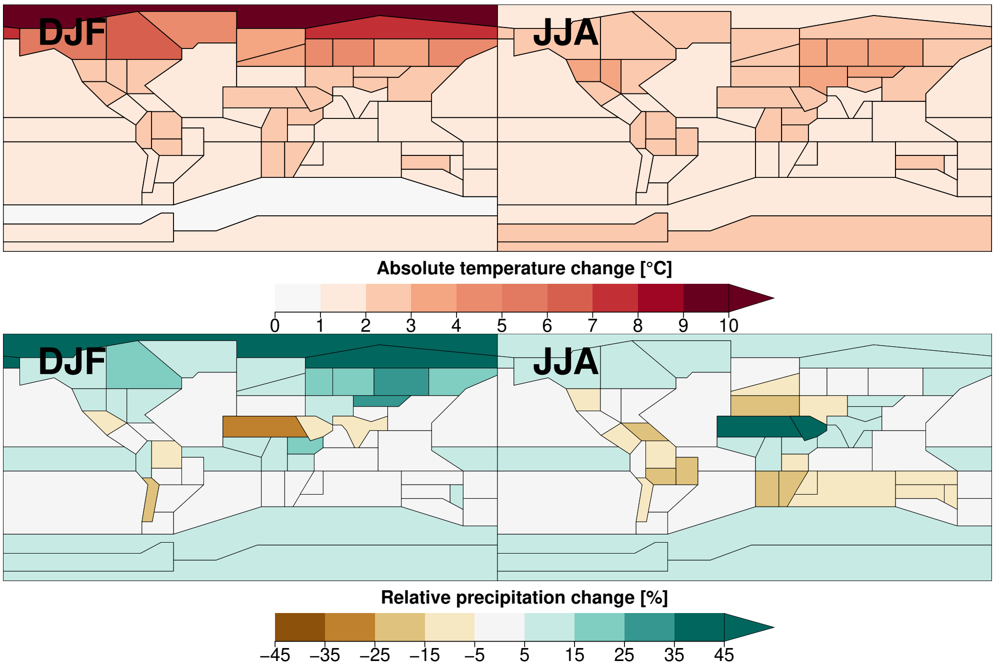

Fig. 2 Mean climate change response at a warming level of +2°C compared with the pre-industrial period (1850–1900), in winter (DJF) and summer (JJA) for absolute changes of temperature (top plots) and relative changes of precipitation (bottom plots).

For both variables and seasons, the most important contribution is related to the disagreement between the GCMs. For 75% of the regions, this contribution exceeds 80% for both temperature and precipitation changes. The contribution of emission scenario uncertainty is remarkably low for both variables, indicating that the climate change responses are close between the different SSP scenarios when expressed as a function of the GWL, in comparison to the GCM uncertainty. Overall, these results support the assumption that the projected changes of seasonal temperature and precipitation can be directly related to the global warming level, at the scale of the AR6 reference region. However, this is likely the case here because we assess changes in atmospheric variables that are less sensitive to the emission pathway (James et al, 2017) in comparison to other regional changes (e.g. sea level, ice cover). This might also be the result of a specific set of 'transient' emission pathways. Using a CMIP5

MME, Pendergrass et al (2015) show that the lowest emission scenario (RCP2.6) leads to higher global precipitation changes per degree in comparison to higher emission scenarios (RCP4.5, RCP6.0, RCP8.5). Stabilized warming patterns obtained on longer periods could also lead to different regional responses if they are impacted by changes with slow feedbacks (e.g. vegetation changes, ice sheets, Collins et al, 2013).

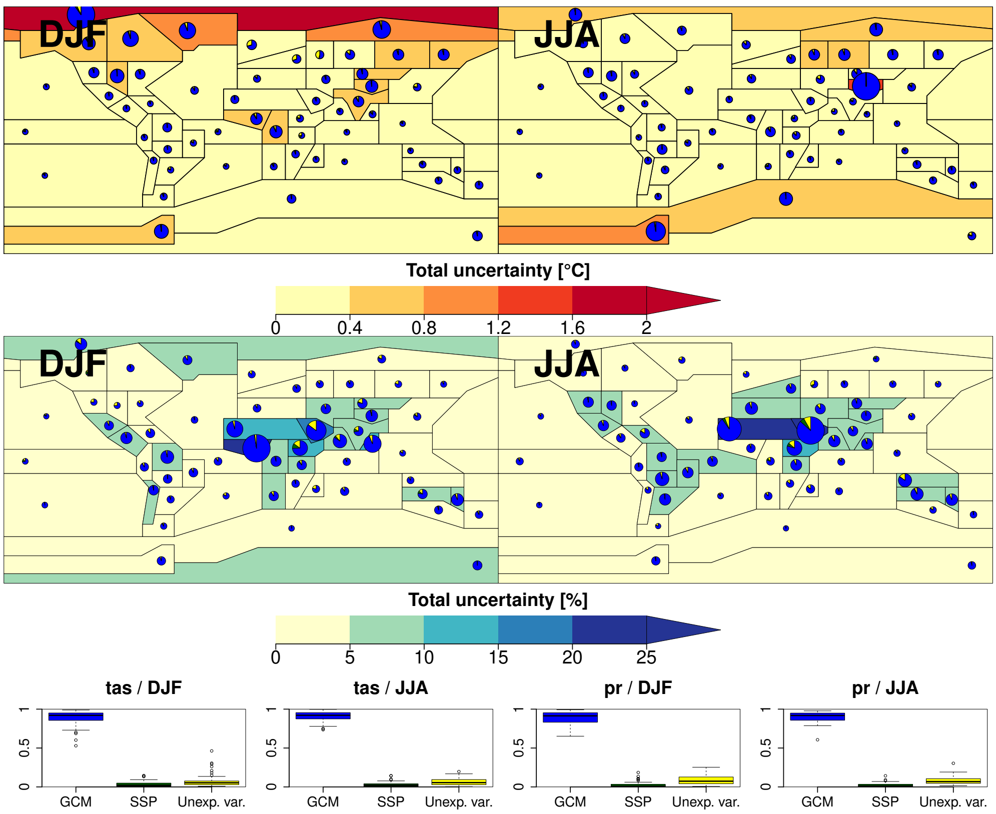

Fig. 3 Total uncertainty $TU(2)$ (square root of the total variance) for absolute changes of mean temperature (tas) and relative changes of total precipitation (pr) in winter (DJF) and summer (JJA) at a warming level of $+2°$C compared with the pre-industrial period (1850–1900). For each reference region, the pie chart provides the contributions of the different components to the total uncertainty (GCM in blue, scenario SSP in green, and unexplained variance in yellow), the radius of the pie chart being a linear function of the total uncertainty. The bottom plots illustrate the dispersion of these proportions over the different reference regions, for each variable and season.

Figure S10 in the Supplement shows the same total uncertainty but at the $1° \times 1°$ resolution. While the spatial patterns are very similar to those shown in Fig. 3, Figure S10 can show large total uncertainties in some specific regions whereas they are small for the corresponding reference region. A striking example concerns the winter precipitation changes in the Equatorial Pacific Ocean (EPO) region where the climate change responses are important for all the GCMs but with different spatial extents (see Fig. S11 in the Supplement). These projected changes in the inter-tropical convergence zone (ICTZ) are roughly consistent between the climate models and between CMIP5 and CMIP6 generations. They indicate a narrowing and strengthening of the ICTZ and greater seasonal precipitation in its core. However, the GCMs do not entirely agree on the extent of the regions where positive precipitation changes are projected. In particular, the areas in the ICTZ with winter precipitation increases are smaller with the GCMs ACCESS-CM2 and UKESM1-0-LL than with the GCMs IPSL-CM6A-LR and MPI-ESM1-2-LR. Another example of greater uncertainty at a $1° \times 1°$ resolution concerns temperature changes in the South of Greenland (Labrador Sea), particularly in winter. The next section describes the GCM uncertainty and details the disagreements between the changes projected by the different GCMs.

5 Spatial variability of GCM uncertainty

Figure 4 presents the GCM uncertainty and the contribution of each GCM to this GCM uncertainty for mean temperature and total precipitation changes in winter and summer. As the GCM uncertainty is the main contributor to the total uncertainty, these maps are similar to those shown in Fig. 3. The GCM uncertainty is directly related to the discrepancies between the different GCM main effects. The largest GCM variances are often due to the effect of one or two GCMs. For example, the contribution of CanESM5 exceeds 75% in the region TIB (Tibet) in summer and 50% in the region GIC (Greenland) in winter. Figs. S12 in the Supplement shows the GCMs with contributions exceeding 50%, for both variables, in winter and summer. For temperature changes, these maps highlight dominant GCM contributions over large areas: CNRM-ESM2-1 in the Arctic Ocean in summer, over Antarctica in winter, MIROC6 in most of North America in winter, and in the ITCZ for both seasons. For precipitation changes, the patterns of dominant GCMs are more patchy but it can be noticed, for example, that MPI-ESM1-2-LR deviates from the other GCMs in North Africa, in summer.

The boxplots of the GCM contributions in Fig. 4 highlight some GCMs that contribute more to the GCM uncertainty than others, e.g. CNRM-ESM2-1, and MIROC6 for winter temperature changes, MIROC6 for summer temperature changes, CanESM5, MIROC6, and MPI-ESM1-2-LR for winter precipitation changes, and MIROC6 and MPI-ESM1-2-LR for summer precipitation changes.

Figure 5 presents the GCM effects, i.e. the deviations between the climate change responses for a GCM and the whole MME. For winter temperature changes, the main GCM effects highlight strong disagreements between the GCMs in the Arctic Ocean, with a difference of 5°C between some GCMs for the same GWL of 2°C. Models ACCESS-CM2, CNRM-ESM2-1, and MPI-ESM1-2-LR lead to more limited warmings in the region than MIROC6. Locally, these maps also show the peculiarities of some GCMs. For example, CanESM5 leads to a much stronger warming than all the other GCMs in Tibet in summer (up to +15°C compared to the other GCMs). Large discrepancies are also obtained in summer over the Southern Ocean which encircles Antarctica. In this region, CanESM5 and UKEMS1-0-LL warm more than MIROC6 and MPI-ESM1-2-LR in summer.

For precipitation changes, large GCM discrepancies can be found in areas where large relative changes are obtained. In Africa, MPI-ESM1-2-LR projects strong negative changes in winter above the equator (see also Fig. S11 in the Supplement) while the other GCMs provide positive changes at least in some regions (in west and east

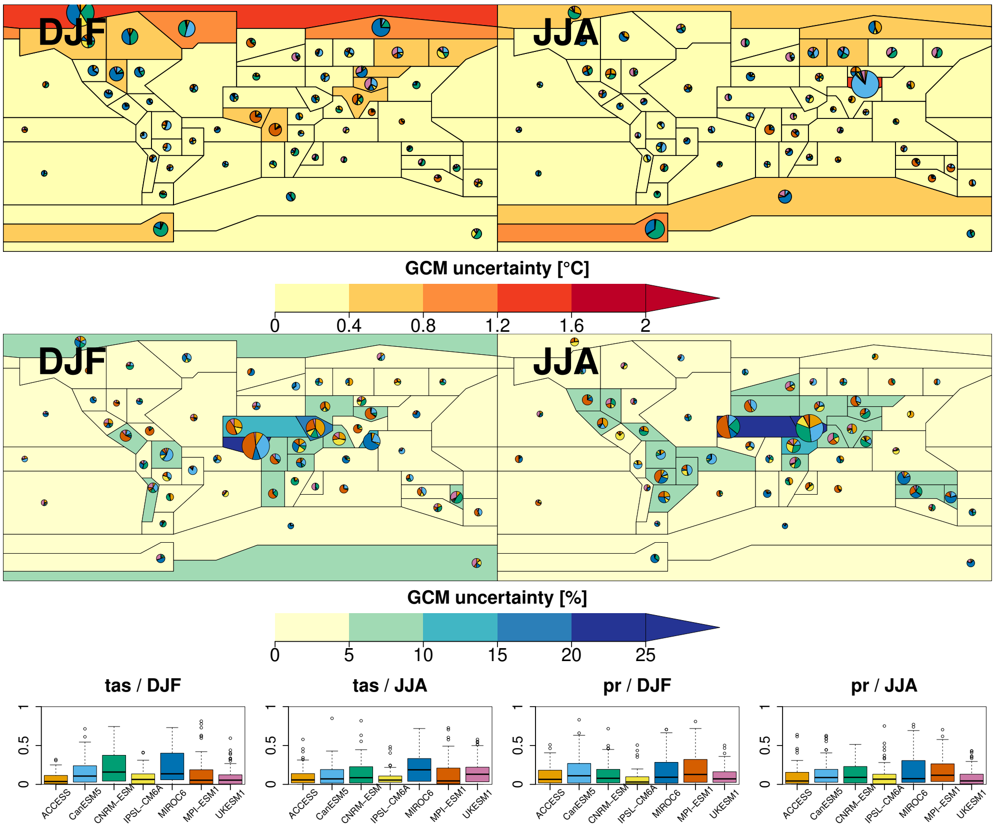

Fig. 4 GCM uncertainty $\sqrt{V_{GCM}(2)}$ (square root of the variance of the main GCM effects) for absolute changes of mean temperature (tas) and relative changes of total precipitation (pr) in winter (DJF) and summer (JJA) at a warming level of +2°C compared with the pre-industrial period (1850–1900). For each reference region, the pie chart provides the contributions of the different GCMs to the GCM uncertainty, the radius of the pie chart being a linear function of the GCM uncertainty. The bottom plots illustrate the dispersion of these proportions over the different reference regions, for each variable and season.

Africa for ACCESS-CM2, in Sub-Saharan Africa above the equator for CanESM5). Similarly, in summer, MPI-ESM1-2-LR leads to the strongest positive changes above the equator in Africa and the Middle East while the other GCMs provide positive changes over smaller regions (west Africa for CanESM5, between the Tropic of Cancer and the equator for all the other GCMs). At the scale of the reference regions, these differences can be up to 100% between the GCMs. For example, in the Arabian

Peninsula, CNRM-ESM2-1, IPSL-CM6A-LR and MPI-ESM1-2-LR lead to large positive summer precipitation changes at a +2°C warming level (+86%, +66%, +59%, respectively) whereas CanESM2 projects negative precipitation changes (-10%).

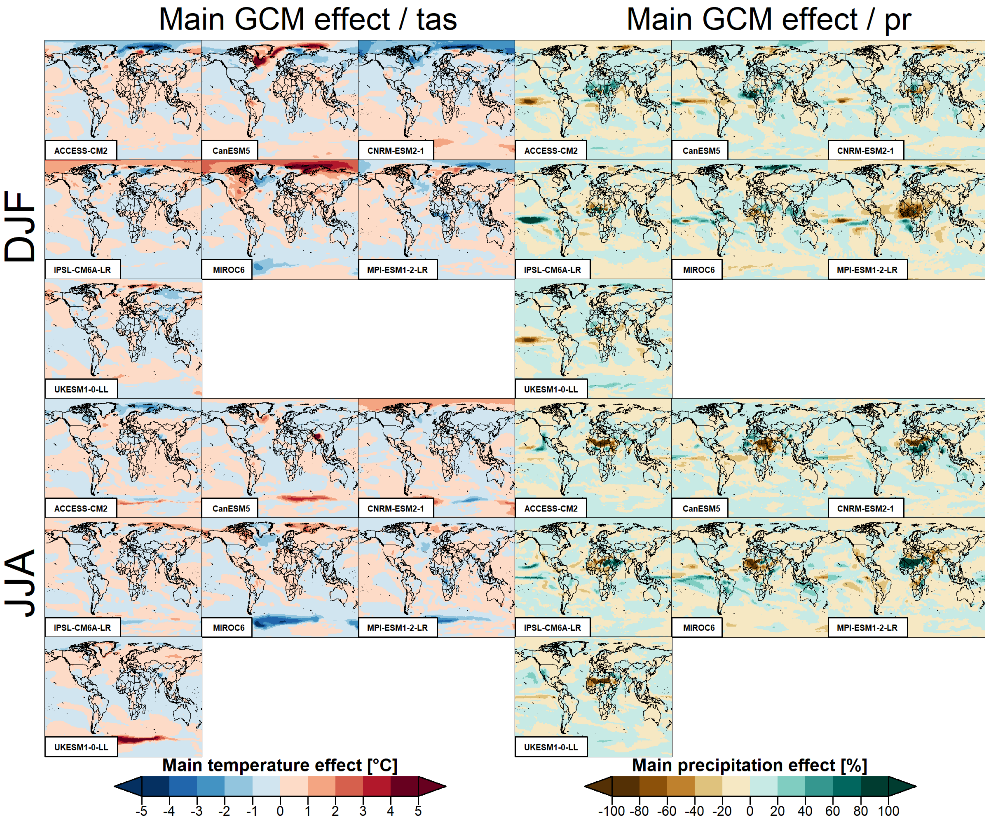

Fig. 5 Main GCM effects at a 1° × 1° resolution for absolute temperature and relative precipitation changes, in winter (DJF) and summer (JJA) at a warming level of 2°C compared with the pre-industrial period (1850–1900).

As indicated in Section 1, many studies have shown that targeting a specific warming level implicitly accounts for the climate sensitivity of the climate models. Smaller GCM uncertainties are thus expected compared to an uncertainty assessment for a given future time, as illustrated in the next Section 6. However, Figures 4 and 5 clearly show that important discrepancies remain between the GCMs for projected changes in regional temperature and precipitation. As shown in Figure 5 and Fig. S11 in the Supplement, regional temperature and precipitation changes are globally similar but differ locally in terms of intensity and spatial extent, especially in some specific regions: the Arctic Ocean and the Southern Ocean for temperature changes, Africa above the equator and the ITCZ area for precipitation changes. Individual evaluations of the GCMs can help to understand these differences (see, e.g. Sigmond et al, 2023, for the model CanESM5).

6 Comparison between uncertainty assessments as a function of global warming and as a function of time

Section 3 presents the method that is applied to obtain uncertainty assessment as a function of the warming level. Here, we perform additional uncertainty assessments as a function of time, i.e. the climate responses, and climate change responses are obtained as a function of time, for the period 1850 to 2100 (the climate response in 1875 being considered as representative of the reference period 1850-1900). The different ANOVA outputs (main effects, variances) are then obtained for each year of this period, for temperature and precipitation changes, and for each reference region.

This comparison between time and warming level uncertainty assessments aims to illustrate the reduction of uncertainties when climate change is considered at a given GWL (similarly to other approaches such as pattern scaling and time sampling). Indeed, it can be expected that removing the discrepancies between the GWL obtained with different emission scenarios (due to different radiative forcings) and GCMs (due to the GCM sensitivity) at the global scale translates into a smaller spread of the climate change responses at the regional scale. This reduction of uncertainties is shown, for example, by Tebaldi et al (2015) with comparisons of annual average surface temperature and precipitation changes in terms of GWL versus radiative forcings. Here, we compare QUALYPSO results obtained for a warming level of +2°C to the QUALYPSO results obtained for 2038, for which the GWL averaged over all SSP scenarios and GCMs is the closest to +2°C (see Figure 1b). The year 2038 is chosen for the sake of illustration and is deemed illustrative of the climate for the near future, although we acknowledge the uncertainty concerning the choice of a specific year. Figures 6 and 7 show the SSP and GCM uncertainties (square root of the variances) for the reference regions when they are obtained for a warming level of 2°C ("GWL") or the mid-century ("Time"), for temperature and precipitation changes, respectively. For both temperature and precipitation changes, SSP uncertainties are lower when uncertainty assessments are performed as a function of the warming level. As discussed above, a smaller SSP uncertainty is expected for these two atmospheric variables, and even becomes non-significantly different from zero for most of the regions (hashed areas), although it can be noticed that the SSP uncertainty is already small for the "Time" assessment in 2038. This is not the case for the following decades, the SSP uncertainty increasing strongly throughout the century (see, e.g., Fig. 1 in Lehner et al, 2020). For temperature changes, the ratio between the SSP uncertainties with the two approaches (Ratio Time/GWL) generally exceeds two, and often four in summer, with a median decrease across the reference regions from 0.09°C to about 0.02°C, for both seasons. For this variable, when applied as a function of the warming level, the climate change responses are strongly in agreement and do not differ too much from one SSP scenario to another. The dispersion of the SSP main effects does not increase strongly as a function of the warming level. When the uncertainty assessments are performed as a function of time, climate change responses exhibit stronger warming for SSP scenarios that lead to the highest radiative forcings (e.g. SSP585). For precipitation changes, the SSP uncertainties are very small (less than 1%) and the difference between "Time" and "GWL" approaches is not pronounced, with significant decreases (hashed areas with the "GWL" approach and not with the "Time" approach, and a ratio greater than two) only for some specific regions (North-East Asia, East Antarctica, North-East North America, Greenland in winter, Southern Ocean, Pacific Ocean, South Asia in summer).

Concerning GCM uncertainties, the comparison between "Time" and "GWL" approaches leads to similar conclusions: they are smaller by a factor of two with the warming level approach for temperature changes and are generally smaller for precipitation changes, especially in some specific regions (high latitudes in winter, Antarctica in summer). In regions where GCM uncertainties are large (e.g. Sahel, Arabian Peninsula) in some areas, as discussed in the previous section. When the uncertainty assessments are performed as a function of time, the ratio "Time/GWL" is often close to one.

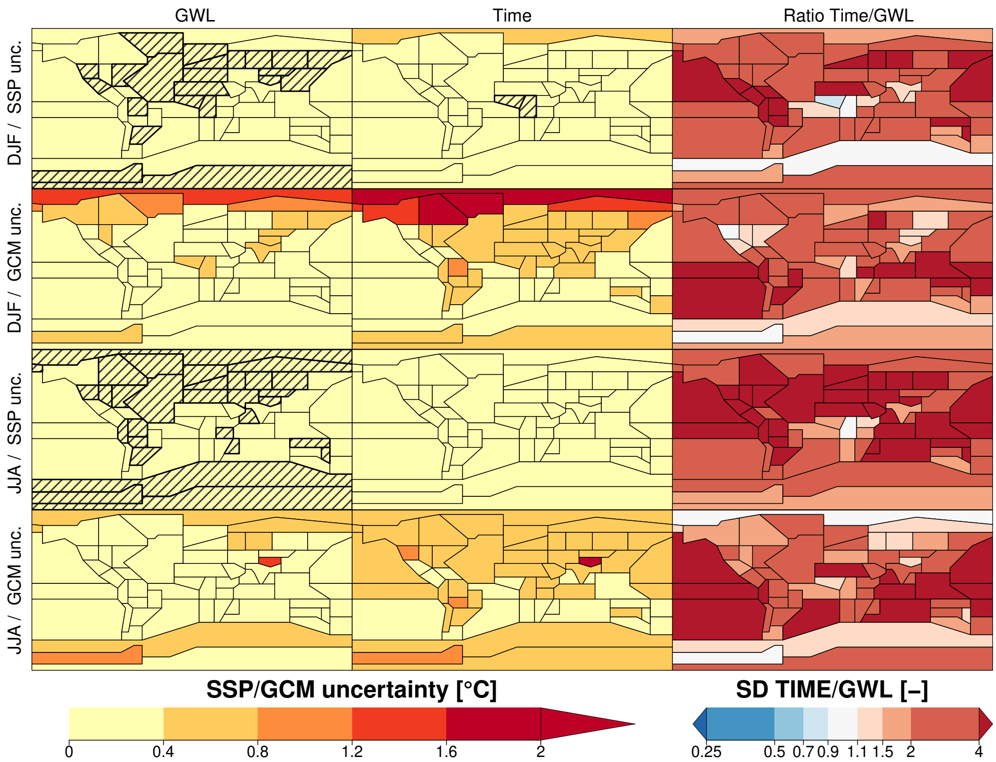

Fig. 6 Uncertainties (square root of the variances) for absolute changes of mean temperature (tas) in winter (DJF) and summer (JJA) when they are obtained for a warming level of 2°C ("GWL") or the year 2038 ("Time") compared with the pre-industrial period 1850-1900. The third column shows the ratio between both uncertainties, e.g. $\sqrt{V_{GCM}(2038)}/\sqrt{V_{GCM}(2)}$ for GCM uncertainties. The first and third lines show the SSP uncertainty $\sqrt{V_{SSP}}$ and the second and fourth lines the GCM uncertainty $\sqrt{V_{GCM}}$. Hashed regions indicate non-significant variances according to the standard F-test of the ANOVA.

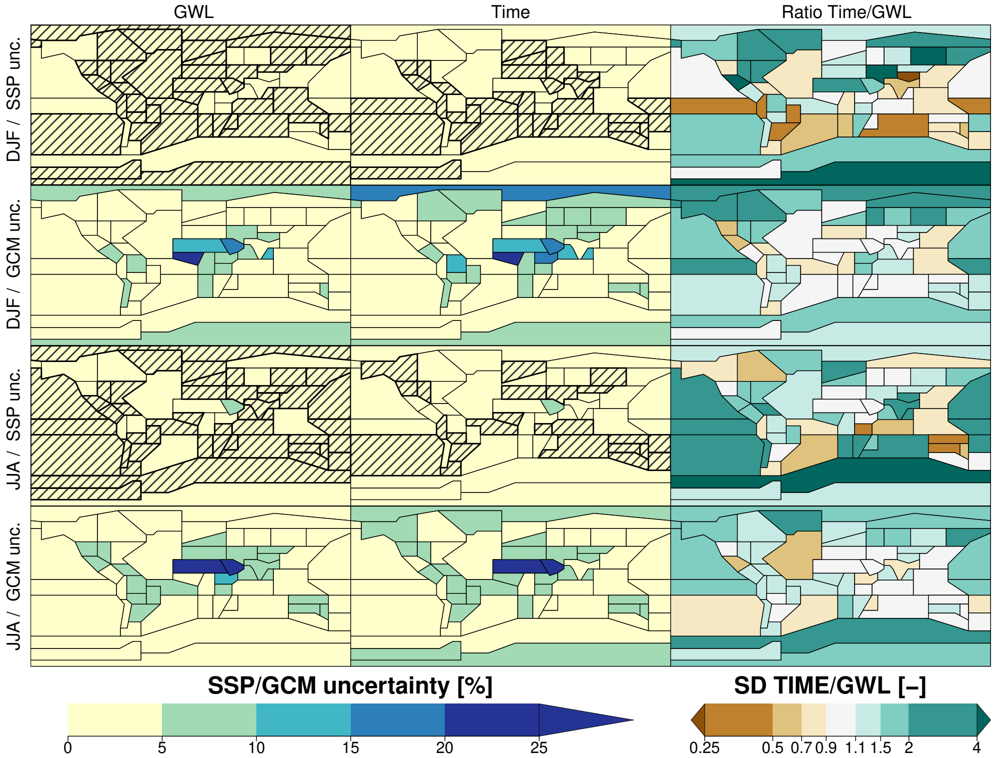

Fig. 7 Same as Figure 6 for relative changes of total precipitation (pr).

7 Discussion and conclusion

This study aims to find the regional climate change response corresponding to a GWL, irrespective of the corresponding time, using an approach consistent with the “pattern scaling" and “time sampling" methods. We first estimate the seasonal temperature and precipitation responses to climate change corresponding to a prescribed GWL, which vary according to the forcing scenario and the GCM. For temperature changes, this approach removes a great part of the uncertainty related to the different pathways taken by the forcing scenario and to the climate sensitivity of each GCM. Concerning precipitation changes, the different uncertainties are only reduced in some specific regions and seasons (high latitudes in winter, low latitudes in summer). This study also shows that the relationship between GWLs and local/regional changes is model-dependent and important uncertainties due to the choice of the GCM remain. For winter temperature changes in the Arctic Ocean, there is a difference of 5°C between the GCMs CNRM-ESM2-1 (colder than the other GCMs) and MIROC6 (warmer than the other GCMs) for the same GWL of +2°C. Similarly, for summer precipitation changes in the Arabian Peninsula, CNRM-ESM2-1 leads to strong positive precipitation changes (+86%) compared to CanESM2 (-10%).

As in many previous studies (James et al, 2017), the warming level is characterized by the annual average of temperature at the planetary scale. The motivation for using these warming levels is that they correlate well with the total amount of GHG emissions which is a main driver of the evolution of the climate system. However, it can also be debated that the warming level should be obtained at a regional scale since it is more directly related to common stakes impacted by climate change (agriculture, forests, water resources, cryosphere, etc.). Indeed, the relationship between the warming level obtained at a global scale and regional climate features can be altered by several mechanisms, e.g. local variations in anthropogenic aerosols forcings (Wei et al, 2021; Persad, 2023).

While the uncertainties of regional temperature (and precipitation changes to a lesser extent) are reduced, this study also highlights some important remaining discrepancies between the responses given by the CMIP6 GCMs. According to some recent studies, the same GCM will not have the same response to the same forcings depending on the speed of their evolutions because the feedbacks are not equivalent. For example, Colman and McAvaney (2009); Gregory and Andrews (2016) show that as climate warms, climate sensitivity weakens, albedo feedback weakens, water vapor feedback strengthens, and lapse rate feedback increases. The understanding of the climate sensitivity of the climate models is an important and open research question that helps the interpretation of the GCM discrepancies (Meehl et al, 2020).

In this study, we do not discuss the important role of internal variability (Lehner and Deser, 2023) which is often the largest contributor to total uncertainty (Hawkins and Sutton, 2011; Evin et al, 2021). Figure Fig. S1a-c in the Supplement illustrates large differences in internal variability from one GCM to another. Therefore, some GCMs probably under/over-estimate the internal variability over the past period. As shown in (Shi et al, 2024, Figure S1), the interannual temperature variability is over-estimated by the CMIP6 GCMs over most of the globe, for both summer and winter seasons. Furthermore, this interannual variability is generally projected to increase at all latitudes in summer and at low latitudes in winter. Concerning seasonal precipitation, the interannual and interdecadal variabilities are generally underestimated by the CMIP6 GCMs (Zhu and Yang, 2021).

MMEs of climate projections are often provided for the next decades using a small selection of emission scenarios as forcings (e.g. CMIP/CORDEX). These MMEs are now exploited to assess climate change as a function of the warming level instead of a future time window. In this study, we show that regional temperature changes are strongly related to the warming level at the planetary scale as represented by the GCMs of the climate projections. This statement also holds for precipitation changes in some specific regions and seasons (North-East Asia, East Antarctica, North-East North America, Greenland in winter, Southern Ocean, Pacific Ocean, and South Asia in summer). We also show that different GCMs can lead to very different regional changes for the same GWL, and it can be expected that it is also the case for variables that are more sensitive to the speed of the changes (biophysical systems, glaciers, ice sheets). In conclusion, these results support the choice of using GWL instead of time in climate change impact studies, as long as the variables of interest are related to seasonal temperature, as it will significantly reduce the range of uncertainties for the projected changes. However, the reduction of uncertainties for variables related to seasonal precipitation is expected to be marginal and vary regionally and seasonally.

Supplementary information. This manuscript has a supplementary file containing additional figures.

Author contribution. GE contributed to the initial version of the study (material preparation, data collection, and analysis). All authors commented on previous versions of the manuscript and approved the final manuscript.

Code availability. Average temperatures at the planetary level and seasonal values at the $1^\circ \times 1^\circ$ grid scale are obtained from GCM simulations using Climate Data Operators (CDO Schulzweida, 2023). The cubic splines are applied with the function `smooth.spline` in R software ({R Core Team}, 2022) with the `df` argument equal to 6. The QUALYPSO package is available at https://cran.r-project.org/package=QUALYPSO.

Data availability. All datasets used in this research can be accessed via the following websites: CMIP6 model outputs at https://esgf-node.ipsl.upmc.fr/projects/cmip6-ipsl/. Access to HadCRUT5 dataset is detailed in Morice et al (2021).

Conflict of interest. The authors have no relevant financial interests to disclose.

References

Baker HS, Millar RJ, Karoly DJ, et al (2018) Higher CO 2 concentrations increase extreme event risk in a 1.5 °C world. Nature Climate Change 8(7):604–608. https://doi.org/10.1038/s41558-018-0190-1

Bichet A, Diedhiou A, Hingray B, et al (2020) Assessing uncertainties in the regional projections of precipitation in CORDEX-AFRICA. Climatic Change 162(2):583–601. https://doi.org/10.1007/s10584-020-02833-z

Brunner L, Pendergrass AG, Lehner F, et al (2020) Reduced global warming from CMIP6 projections when weighting models by performance and independence. Earth System Dynamics 11(4):995–1012. https://doi.org/10.5194/esd-11-995-2020

Collins M, Knutti R, Arblaster J, et al (2013) Long-term Climate Change: Projections, Commitments and Irreversibility. In: Climate Change 2013 - The Physical Science Basis: Contribution of Working Group I to the Fifth Assessment Report of the Intergovernmental Panel on Climate Change. Cambridge University Press, p 1029–1136, URL https://research.monash.edu/en/publications/long-term-climate-change-projections-commitments-and-irreversibil

Colman R, McAvaney B (2009) Climate feedbacks under a very broad range of forcing. Geophysical Research Letters 36(1). https://doi.org/10.1029/2008GL036268

Deser C, Phillips A, Bourdette V, et al (2012) Uncertainty in climate change projections: the role of internal variability. Climate Dynamics 38(3-4):527–546. https://doi.org/10.1007/s00382-010-0977-x

Dosio A, Fischer EM (2018) Will Half a Degree Make a Difference? Robust Projections of Indices of Mean and Extreme Climate in Europe Under 1.5°C, 2°C, and 3°C Global Warming. Geophysical Research Letters 45(2):935–944. https://doi.org/10.

1002/2017GL076222

Evin G, Hingray B, Blanchet J, et al (2019) Partitioning Uncertainty Components of an Incomplete Ensemble of Climate Projections Using Data Augmentation. Journal of Climate 32(8):2423–2440. https://doi.org/10.1175/JCLI-D-18-0606.1

Evin G, Somot S, Hingray B (2021) Balanced estimate and uncertainty assessment of European climate change using the large EURO-CORDEX regional climate model ensemble. Earth System Dynamics 12(4):1543–1569. https://doi.org/10.5194/esd-12-1543-2021, publisher: Copernicus GmbH

Frieler K, Meinshausen M, Golly A, et al (2013) Limiting global warming to 2 °C is unlikely to save most coral reefs. Nature Climate Change 3(2):165–170. https://doi.org/10.1038/nclimate1674

Gregory JM, Andrews T (2016) Variation in climate sensitivity and feedback parameters during the historical period. Geophysical Research Letters 43(8):3911–3920. https://doi.org/10.1002/2016GL068406

Gregory JM, Huybrechts P, Raper SCB (2004) Threatened loss of the Greenland ice-sheet. Nature 428(6983):616–616. https://doi.org/10.1038/428616a

Hawkins E, Sutton R (2009) The Potential to Narrow Uncertainty in Regional Climate Predictions. Bulletin of the American Meteorological Society 90(8):1095–1107. https://doi.org/10.1175/2009BAMS2607.1

Hawkins E, Sutton R (2011) The potential to narrow uncertainty in projections of regional precipitation change. Climate Dynamics 37(1-2):407–418. https://doi.org/10.1007/s00382-010-0810-6

Herger N, Sanderson BM, Knutti R (2015) Improved pattern scaling approaches for the use in climate impact studies. Geophysical Research Letters 42(9):3486–3494. https://doi.org/10.1002/2015GL063569

Hingray B, Saïd M (2014) Partitioning Internal Variability and Model Uncertainty Components in a Multimember Multimodel Ensemble of Climate Projections. Journal of Climate 27(17):6779–6798. https://doi.org/10.1175/JCLI-D-13-00629.1

IPCC (2018) IPCC special report on the impacts of global warming of 1.5 °C above pre-industrial levels and related global greenhouse gas emission pathways, in the context of strengthening the global response to the threat of climate change, sustainable development, and efforts to eradicate poverty. y [V. Masson-Delmotte, P. Zhai, H. O. Pörtner, D. Roberts, J. Skea, P.R. Shukla, A. Pirani, W. Moufouma-Okia, C. Péan, R. Pidcock, S. Connors, J. B. R. Matthews, Y. Chen, X. Zhou, M. I. Gomis, E. Lonnoy, T. Maycock, M. Tignor, T. Waterfield (eds.)], URL http://www.ipcc.ch/report/sr15/, 151pp.

IPCC (2021) Climate Change 2021: The Physical Science Basis. Contribution of Working Group I to the Sixth Assessment Report of the Intergovernmental Panel on Climate Change [Masson-Delmotte, [masson-delmotte, v., p. zhai, a. pirani, s. l. connors, c. péan, s. berger, n. caud, y. chen, l. goldfarb, m. i. gomis, m. huang, k. leitzell, e. lonnoy, j. b. r. matthews, t. k. maycock, t. waterfield, o. yelekçi, r. yu and b. zhou (eds.)] edn. Cambridge University Press, Cambridge, United Kingdom and New York, NY, USA, doi:10.1017/9781009157896

Iturbide M, Gutiérrez JM, Alves LM, et al (2020) An update of IPCC climate reference regions for subcontinental analysis of climate model data: definition and aggregated datasets. Earth System Science Data 12(4):2959–2970. https://doi.org/10.5194/essd-12-2959-2020

James R, Washington R, Schleussner CF, et al (2017) Characterizing half-a-degree difference: a review of methods for identifying regional climate responses to global warming targets. WIREs Climate Change 8(2):e457. https://doi.org/10.1002/wcc.457

Jones PD, New M, Parker DE, et al (1999) Surface air temperature and its changes over the past 150 years. Reviews of Geophysics 37(2):173–199. https://doi.org/10.1029/1999RG900002

Lehner F, Deser C (2023) Origin, importance, and predictive limits of internal climate variability. Environmental Research: Climate 2(2):023001. https://doi.org/10.1088/2752-5295/accf30

Lehner F, Deser C, Maher N, et al (2020) Partitioning climate projection uncertainty with multiple large ensembles and CMIP5/6. Earth System Dynamics 11(2):491–508. https://doi.org/https://doi.org/10.5194/esd-11-491-2020

Lopez A, Suckling EB, Smith LA (2014) Robustness of pattern scaled climate change scenarios for adaptation decision support. Climatic Change 122(4):555–566. https://doi.org/10.1007/s10584-013-1022-y

Mauritzen C, Zivkovic T, Veldore V (2017) On the relationship between climate sensitivity and modelling uncertainty. Tellus A: Dynamic Meteorology and Oceanography 69(1):1327765. https://doi.org/10.1080/16000870.2017.1327765

Meehl GA, Senior CA, Eyring V, et al (2020) Context for interpreting equilibrium climate sensitivity and transient climate response from the CMIP6 Earth system models. Science Advances 6(26). https://doi.org/10.1126/sciadv.aba1981

Mitchell D, AchutaRao K, Allen M, et al (2017) Half a degree additional warming, prognosis and projected impacts (HAPPI): background and experimental design. Geoscientific Model Development 10(2):571–583. https://doi.org/10.5194/gmd-10-571-2017

Morice CP, Kennedy JJ, Rayner NA, et al (2021) An Updated Assessment of Near-Surface Temperature Change From 1850: The HadCRUT5 Data Set. Journal of Geophysical Research: Atmospheres 126(3). https://doi.org/10.1029/2019JD032361

Mulcahy JP, Jones CG, Rumbold ST, et al (2023) UKESM1.1: development and evaluation of an updated configuration of the UK Earth System Model. Geoscientific Model Development 16(6):1569–1600. https://doi.org/10.5194/gmd-16-1569-2023

Nikulin G, Lennard C, Dosio A, et al (2018) The effects of 1.5 and 2 degrees of global warming on Africa in the CORDEX ensemble. Environmental Research Letters 13(6):065003. https://doi.org/10.1088/1748-9326/aab1b1

Paeth H, Vogt G, Paxian A, et al (2017) Quantifying the evidence of climate change in the light of uncertainty exemplified by the Mediterranean hot spot region. Global and Planetary Change 151:144–151. https://doi.org/10.1016/j.gloplacha.2016.03.003

Pendergrass AG, Lehner F, Sanderson BM, et al (2015) Does extreme precipitation intensity depend on the emissions scenario? Geophysical Research Letters 42(20):8767–8774. https://doi.org/10.1002/2015GL065854

Persad GG (2023) The dependence of aerosols' global and local precipitation impacts on the emitting region. Atmospheric Chemistry and Physics 23(6):3435–3452. https://doi.org/10.5194/acp-23-3435-2023

{R Core Team} (2022) R: A Language and Environment for Statistical Computing. Tech. rep., R Foundation for Statistical Computing, Vienna, Austria, URL https://www.R-project.org/

Riahi K, van Vuuren DP, Kriegler E, et al (2017) The Shared Socioeconomic Pathways and their energy, land use, and greenhouse gas emissions implications: An overview. Global Environmental Change 42:153–168. https://doi.org/10.1016/j.gloenvcha.2016.05.009

Ribes A, Boé J, Qasmi S, et al (2022) An updated assessment of past and future warming over France based on a regional observational constraint. Earth System Dynamics 13(4):1397–1415. https://doi.org/10.5194/esd-13-1397-2022

Rigal A, Azaïs JM, Ribes A (2019) Estimating daily climatological normals in a changing climate. Climate Dynamics 53(1):275–286. https://doi.org/10.1007/s00382-018-4584-6

Scafetta N (2021) Testing the CMIP6 GCM Simulations versus Surface Temperature Records from 1980–1990 to 2011–2021: High ECS Is Not Supported. Climate 9(11):161. https://doi.org/10.3390/cli9110161

Schaeffer M, Hare W, Rahmstorf S, et al (2012) Long-term sea-level rise implied by 1.5 °C and 2 °C warming levels. Nature Climate Change 2(12):867–870. https://doi.org/10.1038/nclimate1584

Schleussner CF, Lissner TK, Fischer EM, et al (2016) Differential climate impacts for policy-relevant limits to global warming: the case of 1.5°C and 2°C. Earth System Dynamics 7(2):327–351. https://doi.org/https://doi.org/10.5194/esd-7-327-2016

Schleussner CF, Deryng D, D'haen S, et al (2018) 1.5°C Hotspots: Climate Hazards, Vulnerabilities, and Impacts. Annual Review of Environment and Resources 43(1):135–163. https://doi.org/10.1146/annurev-environ-102017-025835

Schulzweida U (2023) CDO user guide. URL https://doi.org/10.5281/zenodo.10020800

Seneviratne SI, Donat MG, Pitman AJ, et al (2016) Allowable CO2 emissions based on regional and impact-related climate targets. Nature 529(7587):477–483. https://doi.org/10.1038/nature16542

Shi J, Tian Z, Lang X, et al (2024) Projected changes in the interannual variability of surface air temperature using CMIP6 simulations. Climate Dynamics 62(1):431–446. https://doi.org/10.1007/s00382-023-06923-3

Sigmond M, Anstey J, Arora V, et al (2023) Improvements in the Canadian Earth System Model (CanESM) through systematic model analysis: CanESM5.0 and CanESM5.1. Geoscientific Model Development 16(22):6553–6591. https://doi.org/10.5194/gmd-16-6553-2023

Sun C, Jiang Z, Li W, et al (2019) Changes in extreme temperature over China when global warming stabilized at 1.5 °C and 2.0 °C. Scientific Reports 9(1):14982. https://doi.org/10.1038/s41598-019-50036-z

Tebaldi C, Arblaster JM (2014) Pattern scaling: Its strengths and limitations, and an update on the latest model simulations. Climatic Change 122(3):459–471. https://doi.org/10.1007/s10584-013-1032-9

Tebaldi C, Knutti R (2018) Evaluating the accuracy of climate change pattern emulation for low warming targets. Environmental Research Letters 13(5):055006. https://doi.org/10.1088/1748-9326/aabef2

Tebaldi C, O'Neill B, Lamarque JF (2015) Sensitivity of regional climate to global temperature and forcing. Environmental Research Letters 10(7):074001. https://doi.org/10.1088/1748-9326/10/7/074001

Vautard R, Gobiet A, Sobolowski S, et al (2014) The European climate under a 2°C global warming. Environmental Research Letters 9(3):034006. https://doi.org/10.

1088/1748-9326/9/3/034006

Wartenburger R, Hirschi M, Donat MG, et al (2017) Changes in regional climate extremes as a function of global mean temperature: an interactive plotting framework. Geoscientific Model Development 10(9):3609–3634. https://doi.org/https://doi.org/10.5194/gmd-10-3609-2017

Wei L, Wang Y, Liu S, et al (2021) Distinct roles of land cover in regulating spatial variabilities of temperature responses to radiative effects of aerosols and clouds. Environmental Research Letters 16(12):124070. https://doi.org/10.1088/1748-9326/ac3f04

Yip S, Ferro CAT, Stephenson DB, et al (2011) A Simple, Coherent Framework for Partitioning Uncertainty in Climate Predictions. Journal of Climate 24(17):4634–4643. https://doi.org/10.1175/2011JCLI4085.1

Zhu Y, Yang S (2021) Interdecadal and interannual evolution characteristics of the global surface precipitation anomaly shown by CMIP5 and CMIP6 models. International Journal of Climatology 41(S1):E1100–E1118. https://doi.org/10.1002/joc.6756

Supplementary Files

This is a list of supplementary files associated with this preprint. Click to download.

- EvinUncertaintyassessmentCMIP6GWL0402024SM.pdf